The application YAG:Ce³⁺@SiO₂ phosphor for improving color deviation of phosphor-converted light-emitting diode

Thanh Binh Ly[1], Phan Xuan Le[2]
[1]Faculty of Fundamental Science, Industrial University of Ho Chi Minh City, Ho Chi Minh City, Vietnam
[2]Faculty of Mechanical-Electrical and Computer Engineering, School of Engineering and Technology, Van Lang University, Ho Chi Minh City, Vietnam

Article Info	ABSTRACT
	The yellow phosphor $Y_3Al_5O12:Ce^{3+}$ (YAG:Ce³⁺), which sees its most popular use in white light-emitting diode (wLEDs), possess an optical spectrum that lacks the red element. The following article will propose a fresh solution for this problem, which involves adjusting the properties of Ce^{3+} spectrum by using exterior dye particles of ATTO-Rho101, possessing dramatic, wide absorption within the zone of green-yellow spectrum of Ce^{3+} emission and significant release of the red element. The globular YAG:Ce³⁺, which is micrometer and nanometer in size with significant dispersion (micro/nano-YAG:Ce³⁺) was created by employing an altered solvothermal technique. The YAG:Ce³⁺ produced by said technique, along with the heated micro-YAG:Ce³⁺ and commercial phosphors, were exteriorly covered with SiO_2 and immersed in dye at the same time. Effective radiant transmission/reabsorption from Ce^{3+} within the YAG's internal bowel to the dye particles of the exterior hull of SiO_2, regardless of the phosphors' size, was displayed in the YAG: $Ce^{3+}@SiO_{2+}$ dye powder amassed over the stimulation of the light of blue, which boosted the red element of it. The fluorescent microscope was considered an effective device intended for detecting the reabsorption event in grinded substances.

Corresponding Author:

Phan Xuan Le
Faculty of Mechanical-Electrical and Computer Engineering, School of Engineering and Technology,
Van Lang University, Ho Chi Minh City, Vietnam
Email: le.px@vlu.edu.vn

1. INTRODUCTION

Over the decades, such kind of lighting has immensely advanced, which consists of lumen efficiency, great color rendering index (CRI), as well as various advanced attributes [1]-[3]. The creation of the diodes that generate white light-emitting diode (wLED) involves merging the blue, green, and red chips of light-emitting diode (LED), despite that the foundation of most LED lights is phosphor-converted LEDs (pc-LEDs) thanks to the simplicity, quality along with the low cost of the creation process. In this research, we selected an extremely effective organic dye of a rhodamine 101 derivative that can be acquired on the market, and positioned it by covering the surface with silica using an altered Stöber technique and at the same time, immersing in the matrix of SiO_2, upon the exterior of the solvothermally-derived (ethylenediamine) micro/nano-YAG:Ce³⁺ phosphors (~1.0 μm and 10 nm) along with bigger commercial phosphors (~14.8 μm), which subsequently created bowel/hull YAG:Ce³⁺@SiO₂+stain compound phosphors [4]-[6]. The stains possess dramatic and wide absorptivity in the 550-590 nm wavelength range, which is almost identical to the YAG emission, as well as the red element of the spectrum at the wavelength of approximately 609 nm [7], [8]. At all phosphor sizes, instead of the Förster resonance energy transfer

(FRET), the photoluminescence (PL) researches displayed a propagation event of radiative energy, which is the reabsorption process, and used fluorescent microscopy and luminescence degradation dynamics to acquire control of the power reaction between YAG bowel and stain particles of the external hull impacted by blue stimulation [9]-[12]. A fluorescence microscope integrated with an incandescent optic spectrophotometer was proven to be exceptionally effective in detecting the reabsorption event of ground substances through registering the emission spectrum of particles with considerable dispersion on a glass slide and/or a film of conglomerated powder with a shutter is only half-open. In truth, according to our research, the dye, which was stuck in the exterior of the SiO_2 matrix in the micro-YAG:Ce^{3+} after being calcinated, displayed remarkable heat consistency and photo-stability at the temperature of 130 ^{0}C (temperature below such threshold is usually a condition that allows wLED to work). Notably, the defective and/or poorly-attached SiO_2 exterior layer on the bigger commercial phosphors would lower the photo-stability of the dyes placed on such phosphors. We merged the calcinated micro-YAG:Ce^{3+}@SiO_2+stain phosphors with chips that have blue color of LED to create a warm wLED [13]-[15]. When we used the profited YAG:Ce^{3+}@ (SiO_2+dye)$_5$, the R_a of the wLED achieved a mere value of approximately 79, which is caused by the small phosphor concentration scattered within the epoxy resin, followed by the lower reabsorption of the dye particles.

Moreover, we thoroughly specified the compositions, the crystalline formations, the forms along with the luminescence features of the solvothermally-created micro/nano-YAG:Ce^{3+} phosphors. Judging the outcomes, the micro-YAG:Ce^{3+} phosphors have a globular form and can automatically form themselves using tinier nano-particles throughout the solvothermal reaction. In micro/nano-YAG:Ce^{3+}, we detected an interface effect between such nano-particles within the micro-particles and an area influence caused by the greater surface-to-volume scale, respectively [16], [17]. When we follow the yellow radiations, the Ce^{3+} ions exhibit notable widening and blue changes in their stimulation spectrum on the interfaces and surface due to the suitable modifications from 4f to 5d, resulting in a constant wide stimulation range roughly from 300 to 500 nm. Moreover, the Ce^{3+} ions' emissions merely displayed minor blue shifts. As such, said phosphor can be integrated with a chip of LED that generates ultraviolet (UV) lighting to blue lighting. The ability of protonated amine classes (-NH_3^+) to connect with the outer metal ions (Ce^{3+}, Y^{3+}, or Al^{3+}) of the solvothermally generated YAG was demonstrated. They are able to oxidize Ce^{3+} to Ce^{4+} via electron and proton transmission in the event of photoirradiation and heating, and as a result, significantly extinguishing the yellow radiations later covering YAG with a film of SiO_2 or pure YAG nano-particles and after being scattered into the epoxy resin. At the calcination temperature of 1100 ^{o}C, we can eliminate the species on the exterior and boost the phosphors' PL consistency in the event of high temperature and photoirradiance.

2. EXPERIMENTAL DETAILS
2.1. Composition of micro-YAG:Ce^{3+}, nano-YAG:Ce^{3+} and YAG:Ce^{3+}@YAG

We performed every handling in ambient environment. Using an altered technique mentioned above to merge the co-precipitation with a solvothermal procedure which is carried out after, we created the globular YAG:Ce^{3+} phosphors. We used de-ionized water to dissolve suitable portions of Y(NO_3)$_3$ × 6H_2O, Al(NO_3)$_3$ × 9H_2O and Ce(NO_3)$_3$ × 6H_2O for a standard composition, while also attempting to maintain the molar proportion of lanthanide ions (Y^{3+} and Ce^{3+}) to Al^{3+} at 3 : 5. When it came to Ce^{3+}-doped specimens, the Ce^{3+} mol concentration in comparison with the total amount of Y^{3+} and Ce^{3+} ions remained steady at 3%. We back titrated the mother salt combinations into a 0.6 M NH_4HCO_3 ethanol–water (2: 1, v: v ratio) compound at a rate of 2.0 mL min^{-1} with strong stimulation at normal temperature, creating white-color precipitants. After that, we continued to stir the product for 2 hours and then carried out the aging process for 20 hours [18], [19]. After complete cleaning using lots of de-ionized water as well as ethanol, we managed to acquire the precipitate. We used the soggy precipitate to prepare for the following solvothermal reaction through scattering into 70 mL EDA while magnetically stirring. After that, we tightly packed the milky glue scattering (~0.7 g mL^{-1}) into a bottle of 100 mL poly (phenylene oxide) in a pressure cooker made of stainless steel and fired it at 270 ^{o}C within one full day inside a fan oven that had been preheated. Once the autoclave's temperature went down to room level, we separated the precipitate from the mixture by draining the liquid, cleaned it using absolute ethanol, leave it to dry at room temperature in a vacuum oven to obtain the yellow substances, which is YAG powder. For our research, we used the substance as as micro-YAG:Ce^{3+}.

To synthesize the micro-YAG:Ce^{3+}@YAG powder, we utilized a solvothermal reaction as a second step to alter the undoped nano-particles of YAG onto the micro-particles of micro-YAG:Ce^{3+}. We rapidly re-scattered a portion of the previously acquired YAG powder into the EDA solution containing the shapeless co-precipitated precursor of YAG (~0.3 g mL^{-1}). We let the glue scatterings mentioned participate in more solvothermal reaction within an autoclave at the temperature of 270 ^{o}C for a day. Afterwards, we cleaned the

acquired product using absolute ethanol. As it turned out, such co-precipitated YAG forerunners disintegrated and re-crystallized to generate pure YAG nano-particles with diameters of ~100 nm or less, or particles of sub-micro size. A part of the nano-particles have a nucleus in a non-homogenous way, increased in size and formed themselves as quasi-shells located on the exterior of re-scattered micro-particles of micro-YAG:Ce^{3+}, which created the micro-YAG:Ce^{3+}@YAG phosphors. Meanwhile, the other nano-particles having nucleus in a uniform fashion and increased in size in the mixture, with the subsequent event of phase segregation. Such independent nano-particles had inferior size in the range of 5 to 20 nm, and they formed themselves as globular particles with the size of approximately 50 nm to 200 nm. In the article, such independent nano-particles will be called nano-YAG. In order to obtain the micro-YAG:Ce^{3+}@YAG phosphors with increased size and weight at a reduced spinning speed (900 rpm) as a precipitate at the bottom of the pipes, we used a centrifugation speed derived size-isolation approach. We obtained the nano-YAG with inferior size and weight at a greater spinning speed of 3000 rpm in the precipitated mixture. We acquired the nano-YAG from the mixture using more centrifugation at great speed (7000 rpm). We obtained the micro-YAG:Ce^{3+}@YAG:Ce^{3+} and nano-YAG:Ce^{3+} by utilizing the Ce^{3+} doped co-precipitated forerunners in the next solvothermal reactivity. We dried such samples at room temperature in a vacuum oven. The micro-YAG:Ce^{3+} was contained in a quartz tube and heated at the temperature of 1100 ºC for three hours in flowing reducing gas (N$_2$/H$_2$, 95%/5%) so that organic species on the exterior can be eliminated.

2.2. LED fabrication and performance measurements

We used the following components for the job of making wLEDs: solvothermally produced YAG, profited YAG, compound phosphors changed by SiO$_2$ and stain, and blue-color InGaN chips (about 460 nm). We mixed the phosphors with epoxy resin (with a volume proportion of YAG to epoxy resin of ~1:10 to 2:10). We exteriorly covered the chips of LED with the resulting product and heated at the temperature of 120º for twenty minutes in an oven to turn it into a solid substance. The forward current of the operating wLEDs was 20 mA. We determined the photoelectric features of the apparatuses made using an auto-temperatured LED optoelectronic analyzer. To evaluate the YAG photothermal consistency in epoxy resin, we used thermal solidification at 120 °C for 20 minutes to cover a 0.17 mm-thick glass slide with the phosphor-epoxy resin mixture and then placed the glass slide on the heating and cooling phases for measurement.

2.3. Scattering computation

With the Mie theory [20]-[25], we can determine the diffusing factor $\mu_{sca}(\lambda)$, anisotropy factor $g(\lambda)$, and decreased diffusing factor $\delta_{sca}(\lambda)$ with the:

$$\mu_{sca} = \int N(r) C_{sca} (\lambda, r) dr \tag{1}$$

$$g(\lambda) = 2\pi \int \int_{-1}^{1} p(\theta, \lambda, r) f(r) \cos\theta d\cos\theta dr \tag{2}$$

$$\delta_{sca} = \mu_{sca}(1 - g) \tag{3}$$

for the calculations above, $N(r)$ is the dispensation density of diffuse particles (measured in mm^3), C_{sca} represents the scattering cross sections (measured in mm^2), $p(\theta,\lambda,r)$ represents the phase function, λ represents the illumination wavelength (measured in nm), r represents radius of diffuse particles (measured in μm), θ represents the dispersing angle (measured in $°C$), and $f(r)$ represents the dimension distribution function of the diffuser in the phosphorous.

We also generated the micro- YAG:Ce^{3+}@YAG and nano-YAG:Ce^{3+} for the manipulation task using a two-step solvothermal technique. Figure 1 displays their SEM and TEM pictures. As we can see in Figure 1, various nano-particles of YAG with an approximate size of 100 nm are near the exteriors of the YAG:Ce^{3+} micro-particles. As the second solvothermal procedure goes on, the YAG, which was scattered beforehand, yielded various crystal surfaces that became the favorable nucleation locations to house a second growth because of the inferior amount of activation energy. Such locations offer higher chances of nucleation event. The acquired YAG micro-particles shown earlier possessed coarse exteriors and poly-crystallinity, and as such the visible surfaces contain the small pieces detached by the particle limits. Therefore, instead of a constant one-particle shell, the number of nano-particles increased in size on the micro-particles. But the uniform nucleation phenomenon occurred as well. According to Figure 1, various tinier nano-particles of YAG:Ce^{3+}, or nano-YAG:Ce^{3+} when the second reaction employs the Ce^{3+}-doped YAG precipitate precursors, with approximate sizes between 5 and 15 nm were obtained from the supernatant via centrifugation at a low speed of the result of the second solvothermal reaction. The nano-YAG:Ce^{3+}

obviously displayed lattice rims, which suggested the presence of independent crystallinity. The activity of automatic formation expanded to the second reaction system as well. Figure 1 displays a number of globular compositions, which are roughly 50 to 200 nm in sizes. After similar processes, we also infused and exteriorly covered nano-YAG:Ce^{3+} with dye and silica respectively.

Following the calcination process, we infused and exteriorly covered the micro-YAG:Ce^{3+} with dye and silica respectively, which is identical to Figure 1, along with commercial phosphors to boost the red element. Because of the larger dimensions and sleeker exteriors, the growth of SiO$_2$ above the surface of commercialized phosphors became increasingly difficult and sluggish. It was necessary to have five cycles to pinpoint the sufficient amounts of SiO$_2$ and dye particles. According to Figure 2, the chemical alterations created the coarse exteriors with defective and/or poorly-attached layers of SiO$_2$. Through experimentation, it was assumed that the exterior SiO$_2$ layer and the number of dye species failed to rise consecutively as the covering procedure was repeated until it exceeded five cycles.
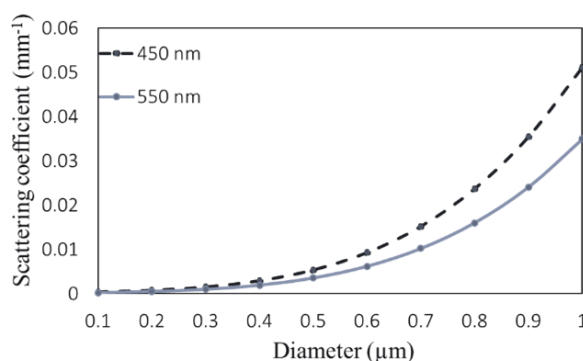

Figure 1. Dispersing factors of SiO$_2$ particles at 450 nm and 550 nm
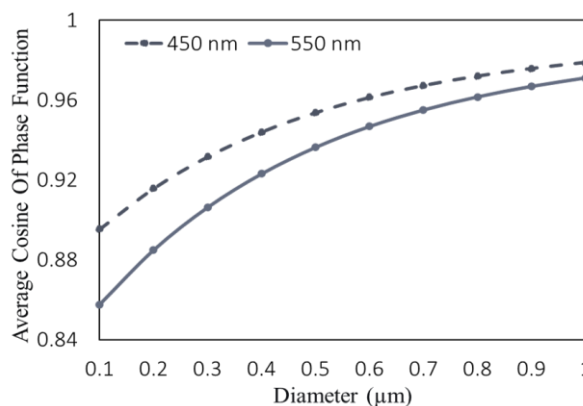

Figure 2. The phase function of SiO$_2$ particles at 450 nm and 550 nm

3.   RESULTS AND DISCUSSION

We can determine the uniformity of the CCT that is subordinate to angle through lowering the highest CCT value to its lowest level. We examined the various masses of SiO$_2$ nano-crystals in order to acquire the most desirable CCT deviation, which can be seen in Figure 3. As usual, the Ce^{3+} stimulation spectrum has two distinct ranges at ~330 and 450 nm owing to electron transfer from the base condition of Ce^{3+} to another region of crystalline dividing the elements of the stimulated 5d condition of Ce^{3+} (^{2}F$_{5/2,7/2}$ → 5d^1 transformations).[2] In Figure 3, this applies the heated micro-YAG:Ce^{3+}, with considerable range among two stimulation ranges. But in the two brand new samples, the bands appeared to considerably widen and lay on each other, which produced a constant wide band between ~300 and 500 nm. Specifically, at the wavelength of approximately 390 nm, there was almost no efficient excitation in the band of colors of the heated micro-YAG:Ce^{3+}, but in the case of micro-YAG:Ce^{3+}, it seemed to be noticeably more potent and was almost identical to the blue band at the wavelength of 450 nm. On the other hand, there was a new band created that yielded an inferior relative intensity in the nano-nano-YAG:Ce^{3+} spectrum. Furthermore, we examined the spectrum's blue shifts of the said samples and saw that the nano-YAG:Ce^{3+} sample had a larger

shift. As the Ce^{3+} ion configuration is 4f, a single electron will advance to a 5d orbital upon the irradiation of UV or blue photon, which renders the 4f hull blank; whereas the closed 5s and 5p electron hulls protects the 4f electrons from the surroundings. Subsequently, the electrons in the 5d orbital have greater sensitivity when spectroscopic is used to examine the changes in the local symmetry. As a result, it is possible for the Ce^{3+} excitation spectrum to directly display the separation data of 5d orbital in the region of crystalline. For the YAG lattice, we merely saw a single D_2 site symmetry for the Ce^{3+} ions; and as such, it is obvious that the widening and the blue shifts have a close relationship with the surface or interface effects because of the particles' insignificant sizes and complicated micro-formation. Because of its significant size of particle as well as tiny BET exterior region, the calcinated micro-YAG:Ce^{3+} hardly altered the size generally but rather abolished the widening effects with great efficiency. Therefore, various interfaces were created along with the tinier nano-units as the micro-particles were integrated with them.
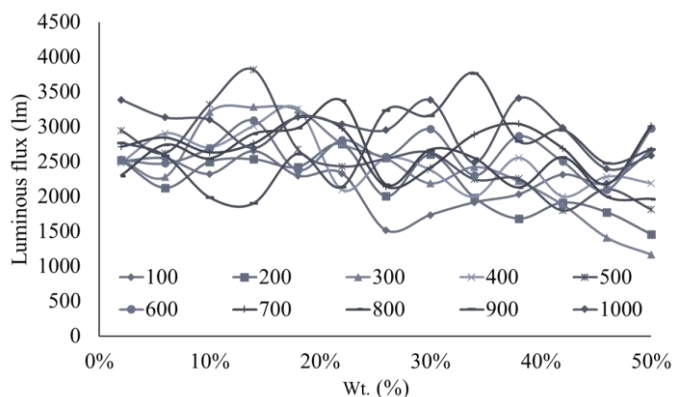

Figure 3. CCT deviations of SiO_2 particles with dissimilar diameters

It is mandatory for the local symmetry to be relaxed and distinct from that of the ions within the particles. In the case of Ce^{3+} located at the interfaces, the highly malformed or jumbled local surrounding could reduce the robustness of the crystal field, leading to a reduction of the direct separation of the 5d orbital and a boost of the 5d electron's inductance power, and subsequently, the excitation transformation from the base condition to the $5d^1$ stimulated condition needed additional power, which is displayed by the excitation band's blue shift along with the occurrence of novel spectral reactions to the significant power aspect of the Ce^{3+} range in the particles. Because nano-YAG:Ce^{3+} has a considerably inferior size and greater exterior region, it is obvious that the occurrence of the new band at the wavelength of approximately 390 nm is caused by the surface influences; but there were not any more notable spectral reactions or more visible blue changes were in comparison to micro-YAG:Ce^{3+}. From this, we can assume that the facade and interface impacts influenced the PL in various ways. The interface effects supported the newly-created excitation band. Furthermore, the exterior effects supported the blue shift of the spectrum. The surface effects with additional exterior faults (such as shattered links) and the species that are exteriorly absorbed (caused by the greater exterior region) along with the greater exterior pressure (caused by the inferior size) seem to be able to twist the local area around the exterior along with the Ce^{3+} internal triggers to alter the crystal field in various ways; and as such the excited situation behaves differently than that caused by interface impacts. Such effects may be able to reduce the direct separation of the 5d orbital and boost the electronic power of the 5d. Hence, the excitation transformation from the base condition to the $5d^1$ stimulated condition and the inversed radiation transformations need additional energy. As a result, we detected additional blue shifts in the blue stimulation range (seen in Figure 4) and also the yellow-green radiation range in nano-YAG:Ce^{3+}.

Judging the emission spectrum in Figure 5, we can see a standard wide Ce^{3+} band of the YAG host matrix, which increases when the wavelength is ~475 to 650 nm and reaches its peak at an approximate wavelength of 500 nm, which is the result of the electron transformations from the 5d's most inferior particle separating element to the base condition Ce^{3+} ($^2F_{5/2}$, $^2F_{7/2}$). As the excitation spectrum displayed its trend, the excitation of the blue band at the wavelength of 455 nm along with the newly-created band at the approximate wavelength of 390 nm in the micro/nano-YAG:Ce^{3+} spectrum displayed a small blue shift, unlike the calcinated micro-YAG:Ce^{3+} spectrum, which is caused by the surface and/or interface effects of Ce^{3+}. In a pattern, the excitation of 390 nm wavelength has a superior blue shift compared to that of 455 mm because the two excitations mostly have according to reaction to various Ce^{3+} ions of the surfaces or interfaces along with the inner ions. The 5d electron's reduced energy cleavage of excited Ce^{3+}, which is

caused by the inferior region of crystalline impacts of the facades/interfaces compared to that of the interior ions and the ensuing boosted the power space from the low-position $5d^1$ stimulated condition to the base condition when excited at the wavelength of 390 nm. In the picture in Figure 5, the bright yellow emission was emitted by micro-YAG:Ce^{3+} along with the extrinsic QY level of approximately 18.1% when excited at the wavelength of 450 nm. Due to the relatively high usual reducing potential of the Ce^{4+}/Ce^{3+} (1.44 V) pair, the EDA particles appeared to decrease the Ce^{4+} ions were at the position of Ce^{3+} during the solvothermal synthesis. In fact, the event in which EDA and oleylamine decreased $Eu^{3+} \rightarrow Eu^{2+}$ was detected earlier throughout the thermolysis and solvothermal reactions. Following the calcination process, the extrinsic QY level was roughly 18.2%.
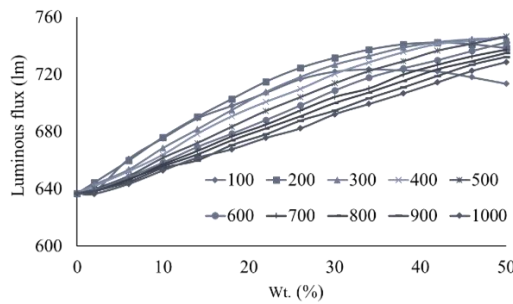

Figure 4. The lumen outputs of the SiO_2 particles with distinct diameters

In Figure 6, we can see the stimulation and radiation spectrum of micro-YAG:Ce^{3+}, micro-YAG:Ce^{3+}@SiO_2 + stain, micro-YAG:Ce^{3+}@(SiO_2 + stain)$_2$ along with the ethanol scatterings of the ATTO-Rho101-APTS conjugate stain. Almost no efficient stimulation displayed the dye in zone of blue spectrum from roughly 400 nm to 500 nm. On the contrary, through tracking the dye's red emission at the wavelength of roughly 615 nm, coupled with the $\pi \rightarrow \pi^*$ electron stimulation of a conjugated carbon-carbon double bond in the stain particle (~270, 550 and 587 nm in UV, green and yellow areas, respectively), the standard wide band in the wavelength range of roughly 300 to 500 nm respective to Ce^{3+} stimulation. Furthermore, it seemed that the two cycles of exterior alterations produced stimulation with twice greater strength in the dye's direct stimulation zone (from roughly 500 nm to 600 nm), while just yielded a minor improvement in the Ce^{3+} ions' mediate stimulation zone, which means that merely a part of dye particles were involved in the activity of energy propagation. Judging the emission spectrum in Figure 6, the red emissions with greater strength (roughly 615 nm) respective to the dye ranges were detected in the patterns with altered exterior when excited into the Ce^{3+} blue band. The emergence and intensification of the dye emissions, which result in the sacrifice of the Ce^{3+} green-yellow emissions, correspond with the features of the activity of the energy propagation; which boosted the red element in the entire spectrum and as a result, becomes highly applicable to the warm wLEDs. Once we re-performed the exterior alteration procedure, the intensity only displayed a minor boost.
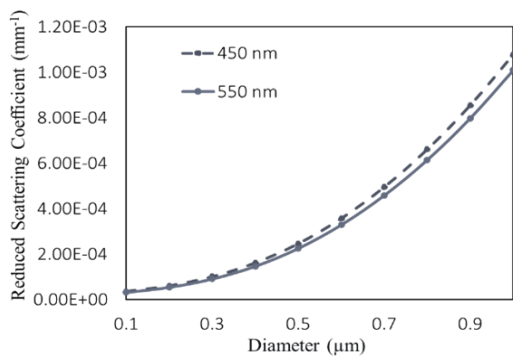

Figure 5. The decreased diffusing factor of SiO_2 particles at dissimilar dimensions and wavelength at 450 nm and 550 nm
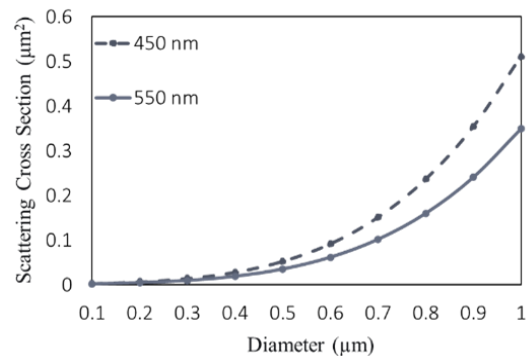
Figure 6. The diffusing cross section of SiO_2 particles at dissimilar dimensions and wavelength at 450 nm and 550 nm

4. CONCLUSION

To sum up, the research examined the synthesis of the globular and hugely-scattered micro-YAG:Ce^{3+} phosphors and nano-YAG:Ce^{3+} nano-particles by using an altered solvothermal technique combined with the procedure of exterior coating with SiO$_2$ and dye-immersing using the ATTO-Rho101 dyes, which also includes the commercial YAG:Ce^{3+} phosphors, in order to boost the red element of the spectrum in the yellow phosphors YAG and make it possible to be applied to warm wLEDs. We considered EDA to be a solvent. It is also the reducing solution used to obtain high PL. The research also thoroughly identified and examined the sizes, forms, crystal formations, compositions, along with the samples' luminescence features. We heated the micro-YAG:Ce^{3+} in order to eliminate the protonated amine species located on the exterior and to compare the PL values. The Ce^{3+} excitation spectrum was demonstrated to be significantly expanded and coupled as a result of the interface/surfaces' relaxed local symmetry, which formed a continuous wide band in the wavelength range of around 300 nm to 500 nm. The interface and facades impacts have varying effects above Ce^{3+} luminescence. While the interface effects of micro-YAG:Ce^{3+} changed the stimulation and luminescence ranges, it had no meaningful impact on the Ce^{3+} dynamics. Furthermore, the exterior influences of nano-YAG:Ce^{3+} had an impact on both. The photo-thermal consistency of micro-YAG:Ce^{3+} luminescence was found to be inferior after exterior alteration with SiO$_2$ or YAG or immersion in an epoxy resin matrix owing to Ce^{3+} → Ce^{4+} oxidation caused by protonated amine types on the exterior when triggered by high temperature or photoirradiation rather than by the oxygen of the surrounding environment. On the contrary, it seemed that the exciting irradiation had greater potency when used to extinguish the PL of micro-YAG:Ce^{3+}. By calcinating at great temperatures, we managed to boost the samples' photo-thermal consistency.

ACKNOWLEDGEMENTS

REFERENCES

[1] X. Yang, M. Zhang, H. Ma, X. Xu, and X. Yu, "Self-Crystallized Ba 2 LaF 7 glass ceramics with high thermal-stability for white light-emitting-diodes and field emission displays," *ECS Journal of Solid State Science and Technology*, vol. 8, no. 10, pp. R127–R132, Oct. 2019, doi: 10.1149/2.0151910jss.

[2] A. Floriduz and J. D. Devine, "Modelling of proton irradiated GaN-based high-power white light-emitting diodes," *Japanese Journal of Applied Physics*, vol. 57, no. 8, p. 080304, Aug. 2018, doi: 10.7567/JJAP.57.080304.

[3] D. T. Khan *et al*., "Study on luminescent properties of Tb3+ and Sm3+ co-doped CaSiO3 phosphors for white light emitting diodes," *Materials Research Express*, vol. 7, no. 1, p. 016507, Jan. 2019, doi: 10.1088/2053-1591/ab5ab8.

[4] C. Chen *et al*., "Flexible inorganic CsPbI3 perovskite nanocrystal-PMMA composite films with enhanced stability in air and water for white light-emitting diodes," *Nanotechnology*, vol. 31, no. 22, p. 225602, May 2020, doi: 10.1088/1361-6528/ab7648.

[5] Y. Zhang, J. Xu, B. B. Yang, Q. Cui, and T. Tian, "Luminescence properties and energy migration mechanism of Eu3+ activated Bi4Si3O12 as a potential phosphor for white LEDs," *Materials Research Express*, vol. 5, no. 2, p. 026202, Feb. 2018, doi: 10.1088/2053-1591/aaab8a.

[6] B. G. Kumar *et al*., "Structural control of InP/ZnS core/shell quantum dots enables high-quality white LEDs," Nanotechnology, vol. 29, no. 34, p. 345605, Aug. 2018, doi: 10.1088/1361-6528/aac8c9.

[7] F. Xu *et al*., "High performance GaN-based hybrid white micro-LEDs integrated with quantum-dots," *Journal of Semiconductors*, vol. 41, no. 3, p. 032301, Mar. 2020, doi: 10.1088/1674-4926/41/3/032301.

[8] Q. Zaman *et al*., "Two-color surface plasmon resonance nanosizer for gold nanoparticles," *Optics Express*, vol. 27, no. 3, p. 3200, Feb. 2019, doi: 10.1364/oe.27.003200.

[9] N. T. Phuong Loan, D. L. Pham, and N. D. Quoc Anh, "Enhancement of color quality scale and luminous flux of white LEDs with remote phosphor geometries*," IOP Conference Series: Materials Science and Engineering*, vol. 617, no. 1, p. 012014, Sep. 2019, doi: 10.1088/1757-899X/617/1/012014.

[10] A. Ali *et al*., "Blue Laser diode-based remote solid-state lighting using plastic optical fiber and phosphor film for a hazardous environment," *ECS Journal of Solid State Science and Technology*, vol. 10, no. 1, p. 016001, Jan. 2021, doi: 10.1149/2162-8777/abd51b.

[11] A. Lenef, M. Raukas, J. Wang, and C. Li, "Phosphor performance under high intensity excitation by InGaN laser diodes," *ECS Journal of Solid State Science and Technology*, vol. 9, no. 1, p. 016019, Jan. 2020, doi: 10.1149/2.0352001jss.

[12] L. Rosso, S. Tabandeh, G. Beltramino, and V. Fernicola, "Validation of phosphor thermometry for industrial surface temperature measurements," *Measurement Science and Technology*, vol. 31, no. 3, p. 034002, Mar. 2019, doi: 10.1088/1361-6501/ab4b6b.

[13] A. K. Dubey, M. Gupta, V. Kumar, V. Singh, and D. S. Mehta, "Blue laser diode-pumped Ce:YAG phosphor-coated cylindrical rod-based extended white light source with uniform illumination," *Laser Physics*, vol. 29, no. 5, p. 056203, May 2019, doi: 10.1088/1555-6611/ab05c0.

[14] F. G. Santamaria, J. E. Murphy, A. A. Setlur, and S. P. Sista, "Concentration quenching in K 2 SiF 6 :Mn 4+ Phosphors," *ECS Journal of Solid State Science and Technology*, vol. 7, no. 1, pp. R3030–R3033, Sep. 2018, doi: 10.1149/2.0081801jss.

[15] A. K. Dubey, V. Kumar, M. Gupta, and D. S. Mehta, "Thermally stable laser-driven phosphor converted white light source using multilayer structured diffuser system," *Laser Physics Letters*, vol. 17, no. 12, p. 126001, Dec. 2020, doi: 10.1088/1612-202X/abc759

[16] Y. H. Kim, N. S. M. Viswanath, S. Unithrattil, H. J. Kim, and W. Bin Im, "Review-phosphor plates for high-power LED applications: challenges and opportunities toward perfect lighting," *ECS Journal of Solid State Science and Technology*, vol. 7, no. 1, pp. R3134–R3147, Oct. 2018, doi: 10.1149/2.0181801jss.

[17] P. S. Dutta, "Full spectrum phosphors for white LEDs and virtual windows for light and health applications," *ECS Journal of Solid State Science and Technology*, vol. 9, no. 1, p. 016023, Jan. 2020, doi: 10.1149/2.0422001jss.

[18] A. Mendieta, B. Fond, P. Dragomirov, and F. Beyrau, "A delayed gating approach for interference-free ratio-based phosphor thermometry," *Measurement Science and Technology*, vol. 30, no. 7, p. 074002, Jul. 2019, doi: 10.1088/1361-6501/ab1b0c.

[19] S. K. Maurya, R. Kushawaha, S. P. Tiwari, A. Kumar, K. Kumar, and J. C. G. E. Da Silva, "Thermal decomposition mediated Er3+/Yb3+ codoped NaGdF4 upconversion phosphor for optical thermometry," *Materials Research Express*, vol. 6, no. 8, p. 086211, May 2019, doi: 10.1088/2053-1591/ab20b4.

[20] H. Feuk, D. Sanned, M. Richter, and M. Aldén, "Sources of error for single-shot PMT-based phosphor thermometry in harsh conditions," *Measurement Science and Technology*, vol. 32, no. 8, p. 084003, Aug. 2021, doi: 10.1088/1361-6501/abfb1e.

[21] L. I. D. J. Martin, D. Poelman, P. F. Smet, and J. J. Joos, "Microscopic study of dopant distribution in europium doped SrGa 2 S 4: Impact on thermal quenching and phosphor performance," E*CS Journal of Solid State Science and Technology*, vol. 7, no. 1, pp. R3052–R3056, Sep. 2018, doi: 10.1149/2.0341709jss.

[22] X. Zhu *et al.*, "Synthesis and Characterization of Er 3+ -Doped SrNb 2 O 6 Phosphor for FIR based thermometer," *ECS Journal of Solid State Science and Technology*, vol. 10, no. 4, p. 046001, Apr. 2021, doi: 10.1149/2162-8777/abf0ea.

[23] E. Hertle *et al.*, "(Gd,Lu)AlO3:Dy3+ and (Gd,Lu)3Al5O12:Dy3+ as high-temperature thermographic phosphors," *Measurement Science and Technology*, vol. 30, no. 3, p. 034001, Mar. 2019, doi: 10.1088/1361-6501/aafcac.

[24] A. Kopf, M. Bardi, E. Kohler, T. Endres, G. Bruneaux, and C. Schulz, "Survivability of the thermographic phosphors YAG:Pr and SMP:Sn in a premixed flame," *Measurement Science and Technology*, vol. 32, no. 7, p. 074001, Jul. 2021, doi: 10.1088/1361-6501/abf57b.

[25] J. Sun, H. Lin, and D. Zhang, "YAG:Ce-Al2O3 composite/spinel dual-layer ceramic phosphor for high luminous density light converting application," *Materials Research Express*, vol. 6, no. 11, p. 116212, Oct. 2019, doi: 10.1088/2053-1591/ab4b0b.

BIOGRAPHIES OF AUTHORS

Binh Thanh Ly (iD) (g) SC (P) received a Environmental Engineering Technology Master degree from the Industrial University of Ho Chi Minh City, in 2020. Currently, He is research Industrial University of Ho Chi Minh City, Vietnam. Her research interests include simulation LEDs material, renewable energy. She can be contacted at email: lythanhbinh@iuh.edu.vn.

Phan Xuan Le (iD) (g) SC (P) received a Ph.D. in Mechanical and Electrical Engineering from Kunming University of Science and Technology, Kunming city, Yunnan province, China. Currently, He is a lecturer at the Faculty of Engineering, Van Lang University, Ho Chi Minh City, Viet Nam. His research interests are Optoelectronics (LED), Power transmission and Automation equipment. He can be contacted at email: le.px@vlu.edu.vn.